JACS
JOURNAL OF THE AMERICAN CHEMICAL SOCIETY

Article

pubs.acs.org/JACS

Simulative and Experimental Characterization of a pH-Dependent Clamp-like DNA Triple-Helix Nanoswitch

Federico Iacovelli,[†,#] Andrea Idili,[‡,#] Alessandro Benincasa,[†] Davide Mariottini,[‡] Alessio Ottaviani,[†] Mattia Falconi,[†] Francesco Ricci,*[,‡] and Alessandro Desideri*[,†]

[†]Department of Biology and [‡]Department of Chemistry, University of Rome, Tor Vergata, 00173 Rome, Italy

Supporting Information

ABSTRACT: Here we couple experimental and simulative techniques to characterize the structural/dynamical behavior of a pH-triggered switching mechanism based on the formation of a parallel DNA triple helix. Fluorescent data demonstrate the ability of this structure to reversibly switch between two states upon pH changes. Two accelerated, half microsecond, MD simulations of the system having protonated or unprotonated cytosines, mimicking the pH 5.0 and 8.0 conditions, highlight the importance of the Hoogsteen interactions in stabilizing the system, finely depicting the time-dependent disruption of the hydrogen bond network. Urea-unfolding experiments and MM/GBSA calculations converge in indicating a stabilization energy at pH 5.0, 2-fold higher than that observed at pH 8.0. These results validate the pH-controlled behavior of the designed structure and suggest that simulative approaches can be successfully coupled with experimental data to characterize responsive DNA-based nanodevices.

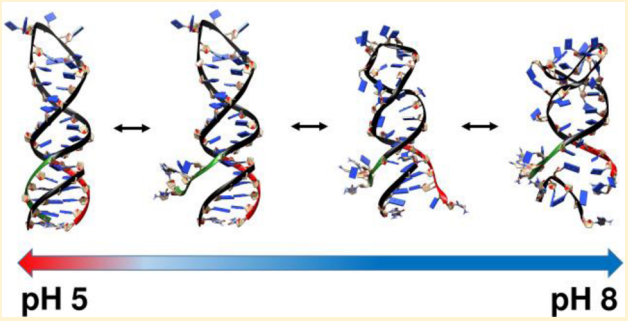

INTRODUCTION

DNA nanotechnology allows us to design and engineer smart nanomaterials and nanodevices using synthetic DNA sequences.[1−6] For example, current methodologies and synthetic strategies, such as DNA tiles, origami, or supramolecular assembly, allowed the production of complex nanostructures of different shapes and dimensions.[7−11] The unparalleled versatility of these approaches allows precise positioning of molecule-responsive switching elements in specific locations of DNA nanostructures, leading to the construction of more complex functional nanodevices.[12−14] Similarly, enzyme−DNA nanostructures have been demonstrated to enhance enzyme catalytic activity and stability.[15] DNA motifs that rely on noncanonical DNA interactions, such as G-quadruplex, triplex, i-motif, hairpin, and aptamers, can be used to design such nanodevices due to their dynamic-responsive behavior toward chemical and environmental stimuli.[16,17] These responsive units often respond to specific chemical inputs through a binding-induced conformational change mechanism that leads to a measurable output or function. The efficiency of this class of responsive nanodevices strongly depends on the designed structure-switching mechanism that controls their activity or functionality. Therefore, there is an urgent need to understand the energies involved in these responsive systems and the relationship between their structure and dynamics.[16]

Among such functional DNA nanodevices, those based on the triple-helix motif are attracting interest for their strong and programmable pH dependence.[18−20] By rationally incorporating triplex-forming portions into DNA nanodevices, it is possible to trigger conformational changes and functions using pH as a chemical input.[21−24] Despite the fair amount of knowledge of the basic design principles and mechanism of action of triplex-based nanodevices, no reports describing the connection between their structural and dynamical properties are available. Toward this aim, simulative approaches represent valuable tools to shed light on the structural, thermodynamic and dynamic properties of DNA nanostructures.[14,25−30] The synergy between experiments and molecular dynamics (MD) simulations may provide significant information for the rational design of functional, pH-activated nanodevices based on a triple-helix motif.

Motivated by the above arguments, here we demonstrate how a combined simulative/experimental approach can be exploited to provide an atomistic description of DNA-based structure-switching mechanisms. As test bed for this study, we have focused on the structural/dynamical behavior of a well-characterized pH-triggered switching mechanism based on the formation of a parallel DNA triple helix[31−35] through a simple two-state clamp-like switching mechanism (Figure 1). The flexibility and modularity of this mechanism permits the fine tuning of the reactivity of different nanomaterials and nanodevices toward pH as demonstrated in recent works.[3,23,24,36] The computational and experimental data presented here indicate that the system is able to form a stable triple helix at pH 5.0, while at pH 8.0 there is no presence of

Received: November 4, 2016
Published: April 2, 2017

DOI: 10.1021/jacs.6b11470
J. Am. Chem. Soc. 2017, 139, 5321−5329

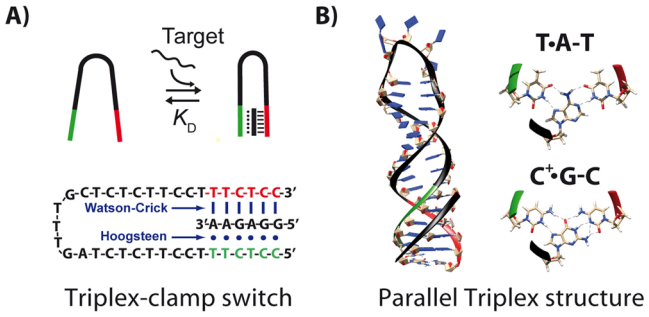

Figure 1. Clamp-like triplex forming DNA nanoswitch here used as a model system: (A) The DNA clamp-like receptor is designed to have a duplex-forming portion (red in the figure) that recognizes through WC interactions a 6-base specific DNA sequence. Such first recognition element is linked, through a random loop (black), to a triplex-forming portion (green) able to recognize the double-stranded DNA and to form a triplex structure composed of both WC and parallel Hoogsteen interactions. (B) Molecular view of the triple-helix structure generated through the formation of the TAT and C^+GC triplets between the clamp-switch and its complementary 6-base DNA strand. C^+GC triplets require the protonation of the N3 of cytosine in the third strand (green) that are therefore stable only at acid pHs (average pK_a of protonated cytosines in triplex structure is ~6.5).[18] On the contrary, TAT triplets are stable at neutral pH and can unfold at higher pHs due to deprotonation of thymine (p$K_a \approx 10$).[20]

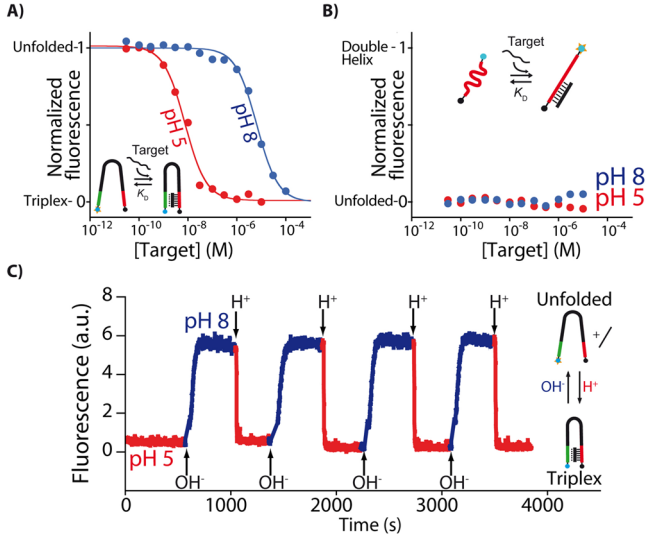

Figure 2. Triplex clamp-switch shows a strong pH-dependent behavior. (A) The affinity of the triplex clamp-switch for its complementary 6-base DNA target is higher at pH 5.0 (red curve) than at pH 8.0 (blue curve). (B) The control linear probe that retains the same WC recognition element of the triplex clamp-switch but lacks the triplex-forming portion is not able to bind the complementary 6-base DNA strand in the same specific target concentration window and at both pHs (red and blue curves). (C) By cyclically changing the pH of a solution containing the triplex clamp-switch and its complementary target from 5.0 to 8.0 we can follow the reversible behavior of the switching mechanism. Here, the binding curves were obtained by adding increasing concentration of a 6-base DNA target to a 10 nM concentration of clamp-switch (A) or control linear (B) in 40 mM Tris buffer, 12.6 mM $MgCl_2$ at the indicated pHs and at 25 °C. For the pH-cycle experiment the solution contains the clamp-switch (10 nM) with the 6-base DNA target (1 μM), and the pH of the solution was cyclically changed by adding small aliquots of 3 M NaOH or HCl in 40 mM Tris buffer, 12.6 mM $MgCl_2$ at 25 °C.

the triple- and even of the double-helical structures. Two accelerated MD (aMD) simulations[37] (500 ns each) of the system, having protonated or unprotonated cytosines mimicking the pH 5.0 and 8.0 conditions, unravelled the atomistic detail of the folded to unfolded transition characterizing the two-state switching mechanism. The present study sets the basis for combined use of experimental and computational approaches to understand the mechanism of novel and efficient nanodevices to be included in complex nanosystems.

EXPERIMENTAL SECTION

Reagents and Materials. All chemicals, including Trizma base (tris(hydroxymethyl)aminomethane), magnesium chloride, hydrochloric acid, sodium hydroxide, and ultrapure urea, were of analytical grade and were purchased from Sigma-Aldrich (St. Louis, MO) unless otherwise indicated.

Oligonucleotides. All oligonucleotide employed in this work were synthesized, labeled, and purified (HPLC and reverse phase) by IBA GmBH (Göttingen, Germany) and used without further purification. Unless otherwise stated, the labeled oligonucleotides were dissolved in Millipore water at a concentration of 1 mM, while the nonlabeled oligonucleotides were dissolved in the relevant buffer (40 mM Tris buffer, 12.6 mM $MgCl_2$, pH 5.0 and 8.0) at a concentration of 100 μM. The final concentration of the oligonucleotides was confirmed using Tecan Infinite M200pro (Männedorf, Switzerland) through a NanoQuant Plate. Before use, each labeled oligonucleotide solution was heated to 95 °C for 5 min and then allowed to cool to room temperature for 2 h. We used a triplex clamp-switch and a linear probe bearing the same recognition element of six bases. These are labeled with Alexafluor 680 (AF680) and Black Hole Quencher 2 (BHQ-2) at the 5′ and 3′ ends. The sequences of the probes were as follows:

Triplex clamp-switch: 5′-*CCTTT*-TCCTTCTCTCGTTTGCTC-TCTTCCT-**TTCTCC**-3′

Linear probe: 5′-CTCTCTTCCT-**TTCTCC**-3′

For the above sequences, the bases in bold represent the duplex-forming portion (red portion in Figures 1 and 2). In the clamp-switch, the underlined bases represent the random loop sequence (black portion in Figures 1 and 2), and the italic bases represent the triplex-forming portion (green portion in Figures 1 and 2). The structure-switching mechanisms of the two probes used in this work are depicted in Figures 1 and 2. Perfect match target was also synthesized and HPLC purified from IBA GmBH (Göttingen, Germany). The sequence of the complementary homopurine 6-base DNA strand was as follows:

Target (6 bases): 5′-GGAGAA-3′

We have also used additional clamp-switches to demonstrate the effect of nonspecific interactions in the kinetic folding and unfolding and to better highlight the role of simulative data. These switches are also labeled with Alexafluor 680 (AF680) and Black Hole Quencher 2 (BHQ-2) at the 5′ and 3′ ends and have the following sequences:

5-base loop triplex clamp-switch: 5′-*CCTCTT*-GTTTG-**TTC-TCC**-3′

12-base target triplex clamp-switch: 5′-*CCTCTTTCCTTC* GTTTG **CTTCCTTTCTCC**-3′

For these sequences, the bases in bold represent the duplex-forming portion, the underlined bases represent the random loop sequence, and the italic bases represent the triplex-forming portion. The perfect match 12-base DNA strand sequence is as follows:

Target (12 bases): 5′-GGAGAAAGGAAG-3′

Binding Curves. All binding curve experiments were obtained using a fixed concentration of the triplex clamp-switch or linear probe (10 nM) and by adding increasing concentrations of a stock solution of the 6-base or 12-base DNA target in a 800 μL volume cuvette. The experiments were conducted in 40 mM Tris buffer, 12.6 mM $MgCl_2$ at different pHs at 25 °C. The fluorescence measurements were obtained using a Cary Eclipse Fluorimeter with excitation at 679 (±5) nm and acquisition between 690 and 712 nm. The fluorescence signals at each target concentration were recorded every 10 min until they reached

DOI: 10.1021/jacs.6b11470
J. Am. Chem. Soc. 2017, 139, 5321−5329

equilibrium. The equilibrated values were fitted to a single-site binding mechanism ([X] = target concentration; F_B = fluorescence in the presence of saturating concentration of target; $F_{[T]}$ = fluorescence in the presence of different concentrations of target; F_0 = background fluorescence):

$$F_{[T]} = F_0 + \left(\frac{[X](F_B - F_0}{[X] + K_D}\right)$$

Kinetic Fluorescence Experiment. The kinetic experiment was performed using a fixed concentration of the triplex clamp-switch (10 nM) in the presence of a saturated amount of 6-base DNA target (1 μM) and at pH 5.0 in a 1400 μL volume stirred cuvette, monitoring the fluorescence signal corresponding to the clamp-switch in the folded triplex state. Successively, the pH of the solution was cyclically changed between pH 8.0 and 5.0 by addition of small aliquots of 3 M NaOH or HCl.

Urea Titration Curve Experiments. Urea titration curves of the triplex clamp-switch in the presence of the DNA complementary target were obtained by sequentially increasing the urea concentration of the buffer solution (40 mM Tris buffer, 12.6 mM $MgCl_2$, pH 5.0 and 8.0) containing the labeled clamp-switch (10 nM) and a saturated amount of the complementary 6-base DNA strand (30 μM) from 0 to 9.5 M. This was achieved by removing small volume of the sample prepared in the working buffer solution and replacing it with a similar volume of clamp-switch (10 nM) and a saturated amount of the complementary 6-base target (30 μM) dissolved in 10 M urea solution and prepared with the same buffer salts (40 mM Tris buffer, 12.6 mM $MgCl_2$, pH 5.0 and 8.0). For each urea concentration, the system was allowed to equilibrate for 3 min prior to measurement. The fluorescence measurements were obtained using a Cary Eclipse fluorimeter with excitation at 679 (±5) nm and acquisition between 690 and 712 nm at a temperature of 25 °C. The fluorescence value at 702 nm (corresponding to the maximum emission of AF680) was used to build the urea titration curves. We determined binding free energies between the clamp-switch and the target strand (at pH 5.0 and 8.0) by fitting the urea titration curves (fluorescence (F) versus urea concentration, [U]) using a two-state unfolding model (see the SI for details)[31,38,39]

$$F = \frac{[T_{tot}](F^\circ_F + \sigma_F[U]) + (F^\circ_{UN} + \sigma_{UN}[U])e^{-(\Delta G^\circ_B(H_2O) - m[U])/RT}}{([T_{tot}] + e^{-(\Delta G^\circ_B(H_2O) - m[U])/RT})}$$

where $\Delta G^\circ_B(H_2O)$ is the binding free energy, m is the dependence of $\Delta G^\circ_B(H_2O)$ on urea concentration (kcal/M·mol), F°_F and F°_{UN} are the fluorescence signals of the folded (bound) and unfolded (unbound) states, respectively, in absence of urea, and σ_F and σ_{UN} represent the dependence of the fluorescence signal of the folded and unfolded states, respectively, on urea concentration. To improve the precision of the fit for the urea titration curve of the clamp-switch in the presence of the DNA target at pH 8.0, we fixed the σ_F value, the dependence of the fluorescence signal of the bound state (triplex state) on urea concentration using the value obtained by linear extrapolation of the initial portion of the curve obtained at pH 5.0 (0.2983 M^{-1}).[31,38,39] While for the urea titration curve of the clamp-switch in the presence of the DNA target at pH 5.0 we fixed the σ_{UN} value, the dependence of the fluorescence signal of the unbound state (unfolded state) on urea concentration using the value obtained by linear extrapolation of the final portion of the curve obtained at pH 8.0 (0.5243 M^{-1}).[31,38,39]

Molecular Dynamics Simulations. The fiber module of the X3DNA program[40] has been used to generate the PDB file template of the triple-helix model, exclusively formed by TAT sequence repetitions. The nucleotide sequence of the strands composing the triple helix has been modified through the X3DNA mutate_bases module[40] in order to match the designed oligonucleotides sequences. The Watson–Crick (WC) strand has been connected to the triplex-forming strand through the sculpting module of the PyMol program[41] to generate the triplex clamp-switch final structure (Figure 1). The structure has been minimized using the UCSF Chimera program[42] to remove any clashes and unwanted interactions introduced by the strands connection modeling. The system topologies and the coordinates of the triple helix at the two pH conditions (i.e., pH 5.0 and 8.0), used as input for the AMBER 14 MD package,[43] have been obtained through the AmberTools tLeap module, parametrizing the structures through the AMBER ff14SB force field[44] with the parmbsc1 corrections.[45] To simulate the pH 5.0 conditions, the residue names of cytosines, composing the triplex-forming strand, were changed according to the AMBER nomenclature for protonated nucleotides. The structures were immersed in a rectangular box filled with TIP3P water molecules,[46] imposing a minimum distance between the solute and the box of 14 Å, and the charges were neutralized adding Mg^{2+} counterions to the solvated systems in favorable positions, as implemented in the tLeap program.[43] For each structure, a minimization run was performed for 2500 steps using the steepest descent algorithm, imposing a harmonic constraint of 50 kcal·mol^{-1}·Å^{-2}, to remove any unfavorable interaction and to prevent irreversible Mg^{2+} binding to DNA. The systems were gradually heated from 0 to 300 K in the NVT ensemble over a period of 500 ps using the Langevin thermostat,[47] with a coupling coefficient of 1.0 ps and a weak constraint of 15 kcal·mol^{-1}·Å^{-2} on nucleotides. At the end of the equilibration phase, the systems were subjected to an equilibrium simulation for 500 ps to remove all constraints. The optimized systems were then simulated using the isobaric–isothermal ensemble (NPT) for 10 ns, using periodic boundary conditions, and a 2.0 fs time-step, using the PME method[48] for the long-range electrostatic interactions with a cutoff of 9 Å for the evaluation of short-range nonbonded interactions. The SHAKE algorithm[49] was used to constrain covalent bonds involving hydrogen atoms. The temperature was fixed at 313 K using the Langevin dynamics,[47] while pressure was held constant at 1 atm through the Langevin piston method.[50] Atomic positions were saved every 500 steps (1.0 ps) for the analyses.

Accelerated Molecular Dynamics Simulations. The classical MD simulations have been carried out to extract the average potential and the average dihedral energies, required by the aMD technique,[37] to modify the potential energy landscape. The aMD technique permits, due to the introduction of a bias potential, access to a large conformational space that cannot be normally accessed by classical MD. The potential modification reduces the local barrier height and allows the calculation to evolve much faster. aMD only requires the evolution of a single copy of the system and does not require any previous knowledge of the potential shape. Each system has been simulated for 500 ns. All simulations were entirely performed using an NVIDIA Tesla K40C GPU.

Trajectory Analysis. Root-mean-square deviations (RMSDs), hydrogen bond time evolution, and PCA analyses have been carried out over the entire 500 ns trajectories by using the GROMACS 4.6.7 analysis tools.[51,52] The hydrogen bond number was evaluated, through the g_hbond module, using an angle cutoff of 30° and a donor–acceptor distance of 3.5 Å. MM-GBSA calculations were performed using the MMPBSA.py code included in the AmberTools distribution.[53] The solvent accessible surfaces were calculated through the CPPTRAJ tool of the AmberTools distribution,[54] while the buried surface areas (BSA) were computed by the formula:

$$BSA = \frac{SAS_{system} - SAS_{clamp\text{-}switch} - SAS_{target}}{2}$$

The reweight of aMD trajectories to recover canonical ensemble and the original free energy profile of the simulated structures has been executed using PyReweighting,[55] a toolkit of python scripts to facilitate the aMD simulation reweighting.

RESULTS AND DISCUSSION

Fluorescence Experiments. The clamp-switch triplex-forming DNA sequence employed here is a 37 base long oligonucleotide comprising two recognition elements of 6 bases (Figure 1, red and green), separated by a loop of 25 bases (Figure 1, black). The switch is labeled with a fluorophore

DOI: 10.1021/jacs.6b11470
J. Am. Chem. Soc. 2017, 139, 5321–5329

(Alexa Fluor 680, AF680) at the 3′ and a quencher (Black Hole Quencher 2, BHQ2) at the 5′ end to follow binding-induced conformational change upon triplex formation. In the presence of its specific DNA target, the switch can fold into a parallel triple helix through a clamp-like mechanism that involves the formation of WC base pairs through the first recognition element (Figure 1, red) and Hoogsteen base pairs through the second recognition element (Figure 1, green). Therefore, the triplex formation induces the closure of the switch leading to the decrease of the fluorescence signal due to the close proximity between AF680 and BHQ2 in the triplex state. Conversely, in the absence of the DNA target, the clamp-switch remains in an open conformation or unfolded state, leading to a high fluorescence signal caused by an increased distance between fluorophore and quencher.

To better highlight the pH-dependence and triplex/duplex transition of the clamp-switch, we employed a short homopurine DNA target composed of six bases, testing the effect of pH in the modulation of the binding mechanism that involves the clamp-switch and its target. Binding curves of the triplex clamp-switch with increasing concentration of the DNA target have been carried out at both pH 5.0 and 8.0 (Figure 2A). The decrease of the signal demonstrates the high affinity of the switch and its ability to effectively bind the short DNA target.[31] As expected, due to the high pH dependence of the parallel Hoogsteen interactions, the dissociation constant achieved at pH 8.0 (i.e., 6.5 ± 0.8 μM) is more than 3 orders of magnitude higher than that observed at pH 5.0 (i.e., 5 ± 1 nM). These findings confirm the importance of the N3 cytosine protonation in the C^+GC triplet formation leading to the overall triple-helix stability (Figure 1B).[18−20]

Such experiments do not provide information regarding the double-helix region and, in particular, if the absence of Hoogsteen base pairs does not permit the formation of the WC base pairs. To investigate the binding mechanism, we employed a control linear probe that retains the same WC recognition element of the clamp-switch and the same fluorophore/quencher couple but lacks the triplex-forming portion. Even at saturating concentrations of the 6-base DNA target we do not observe any signal increase, indicating that the DNA target is not able to bind with the linear probe to form a stable double helix at both pH 5.0 and 8.0 (Figure 2B).

Another important key aspect of a switching-mechanism is its high reversibility. To demonstrate this, we chose a specific concentration of the complementary 6-base DNA strand (1 μM) so that the triplex clamp-switch is able to bind the target at pH 5.0 but not at pH 8.0. We observed a reversible switch from a fully formed triple helix to an unfolded conformation by cyclically varying the pH from 5.0 to 8.0 (Figure 2C). Kinetic analysis of the folding/unfolding processes of the triplex clamp-switch (Figure S1) indicates that unfolding rate (k_u = 0.030 ± 0.002 M^{-1} s^{-1}) is significantly slower than the rate of folding (k_f = 0.24 ± 0.01 M^{-1} s^{-1}). The results indicate that the system is fully reversible and the switching can be monitored several times without any perturbation.

Atomistic aMD Simulations. The atomistic detail of the clamp-switching mechanism has been investigated through aMD simulations, using as a starting structure the computational model described in the Experimental Section. The structure has been simulated with either the protonated or deprotonated N3 cytosines atoms, mimicking the experimental system investigated at pH 5.0 and 8.0, respectively. Both simulations have been carried out for 500 ns, and the two trajectories have been analyzed in a comparative way. The root-mean-square deviation (RMSD), describing the evolution of the sampled conformations in terms of distance from the starting structure, is reported for both the triple (Figure 3A top,

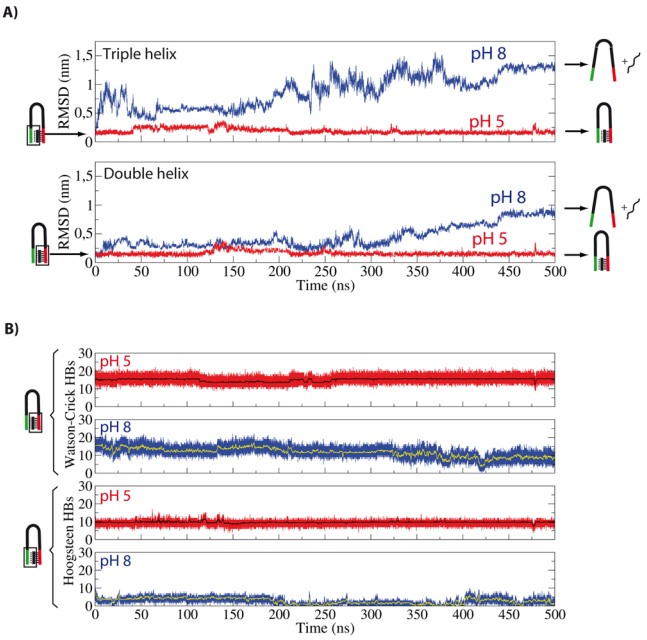

Figure 3. Time-dependent evolution of RMSD and hydrogen-bond number. (A) RMSD of triple-helix region (upper panel) and of the double-helix region (lower panel) belonging to the clamp-switch at pH 5.0 (red line) and 8.0 (blue line), respectively. (B) Evolution of the hydrogen bond number established within the double helix (Watson−Crick panel) and between the double helix and the triplex-forming strand (Hoogsteen panel) at pH 5.0 (red line) and 8.0 (blue line), respectively. The hydrogen-bond numbers, averaged every 100 ps, are highlighted by the black and yellow lines.

pH 8.0 blue line, and pH 5.0, red line) and double helices (Figure 3A bottom, pH 8.0 blue line, and pH 5.0, red line). At pH 5.0 the triple helix is stable, being characterized by small deviations from the starting structure in line with previous simulative data.[56,57] Conversely, at pH 8.0, deviations larger than 1 nm are present (Figure 3A), indicating that the triple helix loses its conformation when the N3 atoms are deprotonated. The RMSD of only the two strands forming the double helix (i.e., the DNA target and the 3′ region of the clamp-switch) gives a similar result. At pH 5.0, the double helix is fully stable, while at pH 8.0 deviations up to 0.8 nm are observed (Figure 3A), indicating that the loss of Hoogsteen interactions also induces the unfolding of the double-helical structure.

Hydrogen Bonds. The number of WC or Hoogsteen hydrogen bonds (HBs) evaluated as a function of time confirms the RMSD results. A constant average number of 10 Hoogsteen HB interactions are observed along the trajectory at pH 5.0, instead of the 12 expected for a regular triple helix containing 3 C−G and 3 A−T base pairs (Figure 3B). This difference is likely due to the flipping of the 5′ terminal guanine of the target oligo that, however, does not alter the stability of the triple helix, preserved during the 500 ns trajectory. Deprotonation of the N3 atoms induces the loss of the Hoogsteen interactions, reducing the number of HBs from 10 to 3 in the first 25 nanoseconds of simulation (Figure 3B). In the remaining part

DOI: 10.1021/jacs.6b11470
J. Am. Chem. Soc. 2017, 139, 5321−5329

of the simulation, the value oscillates between 0 and 4 (Figure 3B), indicating the occurrence of nonspecific interactions in the unfolded structure, as can be noticed upon inspection of different frames as a function of time (data not shown). A similar behavior is observed by monitoring the time-dependent evolution of the WC HBs. A constant average number of 15 HBs is maintained at pH 5.0 (Figure 3B), indicating a high stability of the double-helix region. Conversely, at pH 8.0, the average number of WC HBs is equal to 9 (Figure 3B). This process can be well described by looking both at the persistence of each hydrogen bond evaluated in specific time windows (Figure S2) and measuring the distance of the corresponding base pair as a function of time (Figures 4 and 5). At pH 5.0, all

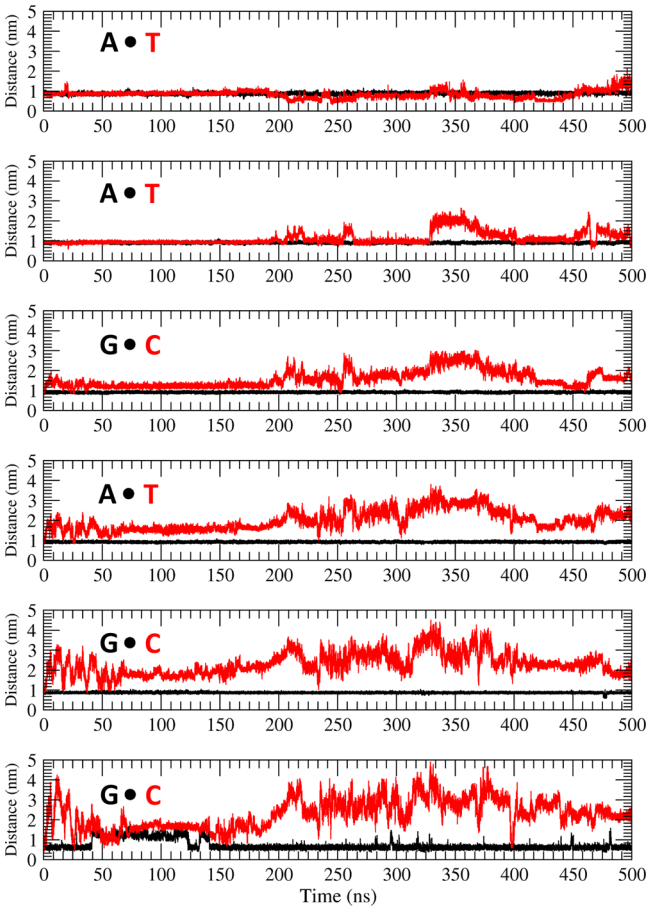

Figure 4. Time dependence of the distance between the mass centers of the base pairs involved in the Hoogsteen interactions calculated at pH 5.0 (black line) and at pH 8.0 (red line).

of the WC and Hoogsteen interactions are maintained in the analyzed time windows, with the exception of the 5′ terminal guanine of the target oligo that loses its Hoogsteen interaction with the cytosine of the switch oligo (Figure S2). This occurs without altering the triple-helix stability. A tricky situation arises at pH 8.0 where the initial four Hoogsteen interactions, starting from the 5′ of the target oligo, are lost in the initial part of the simulation and are never re-established (Figure 4 and Figure S2). The remaining two Hoogsteen interactions are partly maintained in the first 200 ns but are definitively lost in the last part of simulation (Figure 4 and Figure S2).

The loss of the Hoogsteen interactions produces a direct effect on the stability of the WC hydrogen bonds. The

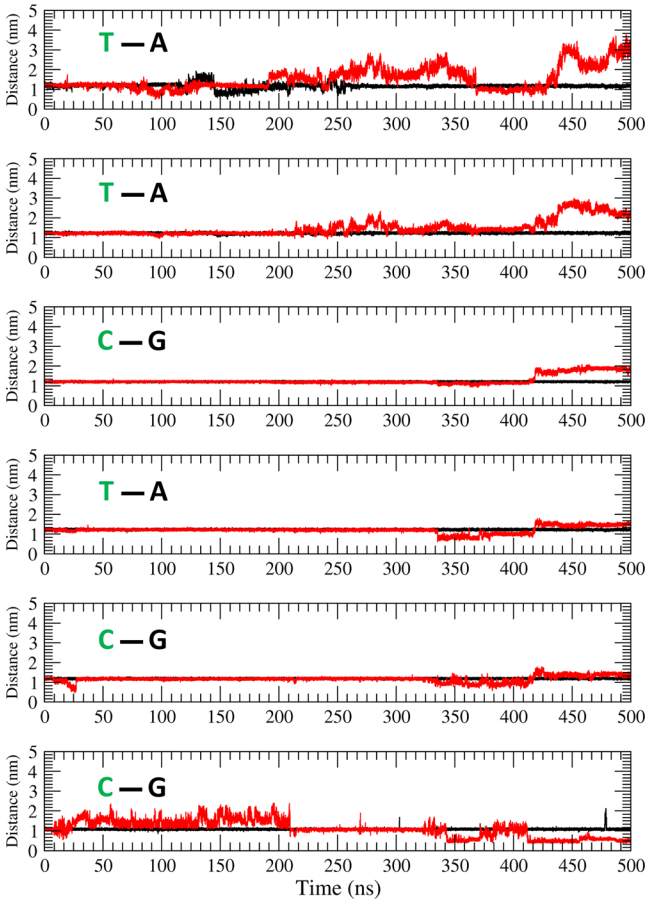

Figure 5. Time dependence of the distance between the mass centers of the base pairs involved in WC HB calculated at pH 5.0 (black line) and at pH 8.0 (red line).

hydrogen bonds established by the central bases of the target oligo are the most stable ones, while the bases at the 5′ and 3′ are the first to be destabilized. With the progress of the simulation, all the WC hydrogen bonds, but one, are entirely lost (Figure 5 and Figure S2). It is interesting to note that at the level of the 5′ an unusual rearrangement is observed involving the 5′ guanine of the target oligo and its base pair partner of the switch oligo. In fact, in the last part of the simulation, the guanine changes orientation, establishing a stacked interaction with the cytosine base pair in the partner oligo that forms two noncanonical hydrogen bonds (Figure S3).

These results provide an atomistic description of the helix dismantling at pH 8.0 and indicate that the designed oligonucleotide sequences permit the occurrence of a stable structure only at low pH, when the presence of the Hoogsteen interactions allows formation of a triple helix, in line with the experiments shown in Figure 2B. This confirms that in the absence of the Hoogsteen contribution the linear probe−target interaction cannot form a stable double-stranded conformation.

Free Energy Projection of the Principal Components of the Motion. As described in the previous paragraph, in the simulations the DNA target never entirely loses the interactions with the clamp-switch even at pH 8.0, where it samples irregular conformations characterized by unusual and partial interactions of the three strands. This behavior can be observed in Figure 6, showing the free energy profile of the sampled conformations at pH 5.0 (right) or 8.0 (left) and reporting the

DOI: 10.1021/jacs.6b11470
J. Am. Chem. Soc. 2017, 139, 5321−5329

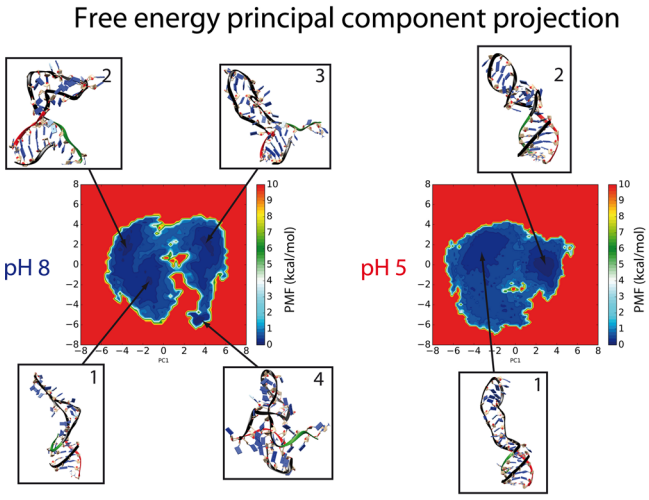

Figure 6. Free energy principal component projection of the system simulated at pH 8.0 (left) and pH 5.0 (right). The numbers 1–4 identify the representative three-dimensional structures corresponding to the low energy long-lived conformations.

representative three-dimensional structures identified in the low-energy basins. At pH 5.0, two main conformations are sampled during the simulation, both characterized by a well-formed triple helix, differing only for the shape of the loop connecting the strands. On the other hand, the conformational sampling at pH 8.0 is wider, and it can be depicted by four main low-energy structures describing the unfolding process of the clamp-switch. In detail, in Figure 6 the low-energy configuration sampled in the first part of the simulation (1), characterized by a structure where the terminal region of the triplex-forming strand starts separating from the double helix, is shown. In the second part (2), the system samples a configuration where the triplex-forming strand is loosely interacting with the double helix through the TAT bases. In the third basin (3), the loss of the interaction with the third strand starts to destabilize the double-helix region, and in the fourth one (4), a complete destabilization of the structure occurs, leading to the formation of irregular unfolded conformations. In the fourth basin (4), it is also possible to observe nonspecific interactions between the 25-base loop portion of the clamp-switch and the target/switch complex, even when the triple helix is fully unfolded. A more in-depth analysis indicates that the nucleotides in the loop can interact with the target-switch complex through stacking interactions and transient hydrogen bonds (Figure S4), providing a possible explanation for the experimentally observed slow unfolding rate. In order to better demonstrate the validity and significance of this approach, we have thus designed a new triplex clamp-switch that presents the same two recognition elements of 6 bases but contains a shorter loop of 5 bases. According to our simulation, this would significantly reduce the nonspecific interactions that are responsible for the slow unfolding rate. The analyses carried out on the aMD simulation of such a 5-base loop clamp-switch clearly indicate the occurrence of a lower number of transient interactions when compared with the 25-base loop clamp-switch. In detail, while the 25-base loop is able to interact with the triplex-forming region through an average number of three hydrogen bonds, reaching the maximum value of seven hydrogen bonds during the simulation time, the 5-base loop only interacts with the triplex-forming region by occasionally establishing one or two hydrogen bonds during all the simulation time (Figure S4). A similar behavior can be observed looking at the number of nonspecific stacking interactions occurring during the unfolding of the clamp-switch systems: we detected 23 stacking interactions for the 25-base loop and 8 for the 5-base loop clamp-switches, respectively (Tables S1 and S2). Moreover, free energy principal component projection identifies low-energy basins in which the loop is not involved in interactions with the triplex portion at pH 8.0 (Figure S5, left), whereas at pH 5.0 the conformational space probed by the clamp-switch is strongly reduced (Figure S5, right). Experimental characterization and kinetic analysis of such clamp-switch confirm that the unfolding rate (0.18 ± 0.03 M^{-1} s^{-1}) becomes significantly faster and comparable to the folding rate (0.42 ± 0.06 M^{-1} s^{-1}) (Figure S6) in line with the reduction of the number of contacts observed in the simulation. This further demonstrates how the atomistic simulation approach provides useful informations for the design and characterization of DNA-based nanodevices.

Energetic Analysis of the Triple-Helix Stability at pH 5.0 and 8.0. To further explore the stability of the triple helix at the two different pH values, urea denaturation experiments have been carried out. This experimental approach allows us to compare the binding free energy of the clamp-switch probe toward the DNA target at different pH values. The urea titration curves of the clamp-switch in the presence of a saturating amount of DNA target (30 μM) at both pH 5.0 and 8.0 reveal a single unfolding transition, occurring at a higher urea concentration at acidic pH compared to that observed at pH 8.0 (Figure 7A). The process is well fitted using a two-state unfolding model[31,38,39] that allows us to obtain the binding free energy of the clamp-switch in absence of urea and therefore estimate the difference in the denaturation process at pH 5.0 and 8.0. The energy difference between the folded and unfolded states of the triple helix corresponds to 12.6 ± 0.1

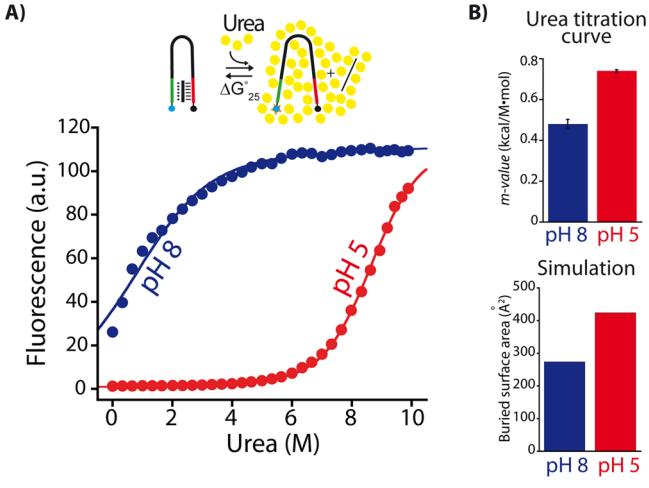

Figure 7. (A) Urea denaturation curves allow estimation of the effect of the pH on the stability of the DNA triple helix formed between the clamp-switch and its 6-base DNA target (at a saturating concentration of 30 μM). As expected, the unfolding/dissociation of the clamp-switch at pH 5.0 (red curve) occurs at higher urea concentrations than pH 8.0 (blue curve), thus confirming the higher stability of the triplex motif at acid pH. (B) *m*-values obtained from the analysis of urea denaturation curves (upper panel) and average values of the buried surface area (lower panel) calculated from the first 50 ns of simulation at the two pHs. Here, the urea denaturation curves were obtained in 40 mM Tris buffer, 12.6 mM $MgCl_2$ at the indicated pHs and at 25 °C.

DOI: 10.1021/jacs.6b11470
J. Am. Chem. Soc. 2017, 139, 5321–5329

kcal/mol at pH 5.0 and 6.6 ± 0.1 kcal/mol at pH 8.0, and so the $\Delta\Delta G$ between the two different pH values corresponds to 6.0 ± 0.2 kcal/mol. These results confirm the effect of the protonated cytosines that provide, at pH 5.0, an additional stabilization energy two times larger than that observed at pH 8.0.

The stability of the triple helices at the two different pH values has been also evaluated through the MM/GBSA approach by analyzing the first 50 ns of the aMD trajectories, where the system maintains the triple helical structure even at pH 8.0. These data indicate that at pH 5.0 the clamp-switch/target interaction is characterized by an energy value of −92.3 kcal/mol that is almost twice that observed at pH 8.0 where the value decreases to −50.5 kcal/mol. The absolute values obtained from the experimental and simulative approaches are not directly comparable, due to the simulative approximations, but they both converge in assigning to the state at pH 5.0 an interaction energy almost 2-fold higher than that observed at pH 8.0.

Another interesting point concerns the ratio of the *m* values, obtained by the urea unfolding experiments, that correlates well with the ratio of the amount of BSA evaluated for the simulated systems at pH 8.0 and 5.0. As reported in Figure 7B, the BSA detected at pH 5.0 is about 1.55 times larger than that observed at pH 8.0, in agreement with the experimental *m* value ratio (1.60). The *m* values have been reported to be strongly correlated with the amount of solvent accessible surface being proportional to the number of denaturant molecules that can access the interface.[58] The calculation at atomistic level of the BSA, evaluated for the simulations at the two pHs, confirms the strict correlation between these two parameters and provide a structural explanation for the different behavior of the system at the two pH conditions.

Simulative Approach To Design New DNA-Based Switching Devices. To further demonstrate the strength of the concomitant use of both the simulative and experimental approaches and show how simulative results can guide the design of new DNA-based nanodevices, we have studied a clamp-switch system having a different pH behavior. We wanted to demonstrate that it is possible to use simulation data to design a clamp-switch that, contrary to the one we described previously, presents a stable duplex conformation at both pH 5.0 and 8.0 and only shows pH-induced transition from the triplex to the duplex state. Our simulative data show that such behavior could be obtained by using a clamp-switch containing a pair of 12-base recognition elements (both duplex- and triplex-forming elements) and a 5-base loop in association with a target of 12 bases. Both RMSD analysis (Figure S7) and hydrogen-bond evolution (Figure S8) for such a system predict that while the duplex helix portion is maintained for all of the simulation time at both pH 5.0 and 8.0 (similar to the behavior of the triple helix at pH 5.0), the triple helix is rapidly destabilized at pH 8.0. MM/GBSA calculations indicate that the energy value of the clamp-switch/target interaction at pH 5.0 (−213.9 kcal/mol) is almost twice that observed at pH 8.0 (−112.8 kcal/mol). The experimental results support the simulative data and show a highly stable duplex state (Figure S9) and a ratio between the free energies at pH 5.0 and pH 8.0 obtained with urea denaturation experiments similar to those achieved with our simulation (Figure S10).

CONCLUSION

The experimental and simulative data reported here represent a first attempt to characterize and describe at the atomistic level the switching mechanism of a DNA-based nanodevice specifically designed to respond to pH changes. The simulative data indicate that at pH 5.0 the Hoogsteen interactions are able to confer a high stability to the structure that is well maintained for all the 500 ns of simulation time. Cytosine deprotonation at high pHs induces a fast unfolding process, due the loss of the Hoogsteen and then of the WC interactions, preventing to ensure a stable structure. The simulative approach allows us to observe, from a dynamic point of view, the evolution of the hydrogen bond network, indicating that at pH 8.0 the four Hoogsteen interactions are immediately lost (Figure 4 and Figure S2). The successive loss of the remaining two Hoogsteen interactions has a direct effect on the stability of the WC hydrogen bonds. The triplex-forming strand disassembly promotes the sampling of a large number of unstable conformations, but despite the significant conformational changes, the close proximity of the clamp and target DNA observed in the simulations permits the structure to reversibly switch from the unfolded to folded state every time the pH is changed as demonstrated by the fluorescence experiments (Figure 2C). Additionally, the simulative approach allows us to describe the presence of nonspecific interactions between the loop and the switch-target complex and to better describe the kinetic behavior of the triplex clamp-switch. This information, which would have been difficult to achieve with experimental data, has been employed to improve the design of the clamp-switch and to achieve faster unfolding kinetics. Finally, urea-unfolding experiments and MM/GBSA calculations carried out on the first 50 ns of simulation converge in observing a stabilization energy at pH 5.0 twice that at pH 8.0, shedding light on the energy contribution of the additional Hoogsteen hydrogen bonds in preserving the triple-helical conformation. All of these data validate the behavior of the designed structure and suggest that simulation approaches can be successfully coupled with experimental data to characterize responsive DNA-based nanodevices.

DNA-based nanodevices are usually designed employing user-friendly softwares (i.e., Mfold,[58] NUPACK,[59] etc.) which allow us to accurately predict the thermodynamics of Watson−Crick interactions. However, these tools inevitably fail to predict energies of DNA-based nanodevices where non-canonical interactions are involved. In response to this limitation, we demonstrate here that simulative approaches can help in the optimization of DNA-based nanodevices controlled by pH changes that have been recently proposed for both diagnostic and drug-delivery applications.[20,23,24] Moreover, the simulation approaches we have employed here might help in the characterization of response time and prediction of the effect of environmental conditions which obviously represent crucial factors in the performance of such DNA-based tools. Finally, we note that, while we have focused here on DNA-based switches controlled by pH, the applicability of simulation approaches in the field of DNA nanotechnology could be expanded to other noncanonical DNA structures (i.e., i-motif, G-quadruplex, etc.), to more complex systems (i.e., aptamers, DNAzymes, etc.) and to DNA nanodevices modified with different chemical groups.

DOI: 10.1021/jacs.6b11470
J. Am. Chem. Soc. 2017, 139, 5321−5329

■ ASSOCIATED CONTENT

Supporting Information

The Supporting Information is available free of charge on the ACS Publications website at DOI: 10.1021/jacs.6b11470.

Urea fitting equation and supplementary figures (PDF)

■ AUTHOR INFORMATION

Corresponding Authors

*francesco.ricci@uniroma2.it

*desideri@uniroma2.it

ORCID

Andrea Idili: 0000-0002-6004-270X

Francesco Ricci: 0000-0003-4941-8646

Author Contributions

#F.I. and A.I. contributed equally.

Notes

The authors declare no competing financial interest.

■ ACKNOWLEDGMENTS

This work was supported by Associazione Italiana per la Ricerca sul Cancro, AIRC (Project No. 14420) (FR), by the European Research Council, ERC (Project No. 336493) (FR), by the Italian Ministry of University and Research (Project of National Interest, PRIN, 2012 CTAYSY), and by the NVIDIA Corporation (donation of Tesla K40C to M.F.).

■ REFERENCES

(1) Um, S. H.; Lee, J. B.; Park, N.; Kwon, S. Y.; Umbach, C. C.; Luo, D. *Nat. Mater.* **2006**, *5*, 797.

(2) Kuzyk, A.; Schreiber, R.; Fan, Z.; Pardatscher, G.; Roller, E.-M.; Högele, A.; Simmel, F. C.; Govorov, A. O.; Liedl, T. *Nature* **2012**, *483*, 311.

(3) Huang, F.; Liao, W. C.; Sohn, Y. S.; Nechushtai, R.; Lu, C. H.; Willner, I. *J. Am. Chem. Soc.* **2016**, *138*, 8936.

(4) Liu, W.; Halverson, J.; Tian, Y.; Tkachenko, A. V.; Gang, O. *Nat. Chem.* **2016**, *8*, 867.

(5) Ke, Y.; Meyer, T.; Shih, W. M.; Bellot, G. *Nat. Commun.* **2016**, *7*, 10935.

(6) Langecker, M.; Arnaut, V.; Martin, T. G.; List, J.; Renner, S.; Mayer, M.; Dietz, H.; Simmel, F. C. *Science* **2012**, *338*, 932.

(7) Winfree, E.; Liu, F.; Wenzler, L. A.; Seeman, N. C. *Nature* **1998**, *394*, 539.

(8) Wei, B.; Dai, M.; Yin, P. *Nature* **2012**, *485*, 623.

(9) Rothemund, P. W. K. *Nature* **2006**, *440*, 297.

(10) Douglas, S. M.; Marblestone, A. H.; Teerapittayanon, S.; Vazquez, A.; Church, G. M.; Shih, W. M. *Nucleic Acids Res.* **2009**, *37*, 5001.

(11) McLaughlin, C. K.; Hamblin, G. D.; Aldaye, F. a; Yang, H.; Sleiman, H. F. *Chem. Commun.* **2011**, *47*, 8925.

(12) Andersen, E. S.; Dong, M.; Nielsen, M. M.; Jahn, K.; Subramani, R.; Mamdouh, W.; Golas, M. M.; Sander, B.; Stark, H.; Oliveira, C. L. P.; Pedersen, J. S.; Birkedal, V.; Besenbacher, F.; Gothelf, K. V.; Kjems, J. *Nature* **2009**, *459*, 73.

(13) Douglas, S. M.; Bachelet, I.; Church, G. M. *Science* **2012**, *335*, 831.

(14) (a) Juul, S.; Iacovelli, F.; Falconi, M.; Kragh, S. L.; Christensen, B.; Frøhlich, R.; Franch, O.; Kristoffersen, E. L.; Stougaard, M.; Leong, K. W.; Ho, Y. P.; Sørensen, E. S.; Birkedal, V.; Desideri, A.; Knudsen, B. R. *ACS Nano* **2013**, *7*, 9724. (b) Franch, O.; Iacovelli, F.; Falconi, M.; Juul, S.; Ottaviani, A.; Benvenuti, C.; Biocca, S.; Ho, Y.-P.; Knudsen, B. R.; Desideri, A. *Nanoscale* **2016**, *8*, 13333.

(15) (a) Zhao, Z.; Fu, J.; Dhakal, S.; Johnson-Buck, A.; Liu, M.; Zhang, T.; Woodbury, N. W.; Liu, Y.; Walter, N. G.; Yan, H. *Nat. Commun.* **2016**, *7*, 10619. (b) Gao, Y.; Roberts, C. C.; Toop, A.; Chang, C. A.; Wheeldon, I. *ChemBioChem* **2016**, *17*, 1430−1436.

(16) Yatsunyk, L. A.; Mendoza, O.; Mergny, J. L. *Acc. Chem. Res.* **2014**, *47*, 1836.

(17) Wang, F.; Liu, X.; Willner, I. *Angew. Chem., Int. Ed.* **2015**, *54*, 1098.

(18) Leitner, D.; Schröder, W.; Weisz, K. *Biochemistry* **2000**, *39*, 5886.

(19) Sugimoto, N.; Wu, P.; Hara, H.; Kawamoto, Y. *Biochemistry* **2001**, *40*, 9396.

(20) Idili, A.; Vallée-Bélisle, A.; Ricci, F. *J. Am. Chem. Soc.* **2014**, *136*, 5836.

(21) Chen, Y.; Lee, S. H.; Mao, C. *Angew. Chem., Int. Ed.* **2004**, *43*, 5335.

(22) Han, X.; Zhou, Z.; Yang, F.; Deng, Z. *J. Am. Chem. Soc.* **2008**, *130*, 14414.

(23) Porchetta, A.; Idili, A.; Vallée-Bélisle, A.; Ricci, F. *Nano Lett.* **2015**, *15*, 4467.

(24) Idili, A.; Porchetta, A.; Amodio, A.; Vallée-Bélisle, A.; Ricci, F. *Nano Lett.* **2015**, *15*, 5539.

(25) Yoo, J.; Aksimentiev, A. *Proc. Natl. Acad. Sci. U. S. A.* **2013**, *110*, 20099.

(26) Yoo, J.; Aksimentiev, A. *J. Phys. Chem. Lett.* **2015**, *6*, 4680.

(27) Maffeo, C.; Yoo, J.; Aksimentiev, A. *Nucleic Acids Res.* **2016**, *44*, 3013.

(28) Iacovelli, F.; Alves, C.; Falconi, M.; Oteri, F.; De Oliveira, C. L. P.; Desideri, A. *Biopolymers* **2014**, *101*, 992.

(29) Alves, C.; Iacovelli, F.; Falconi, M.; Cardamone, F.; Morozzo Della Rocca, B.; De Oliveira, C. L. P.; Desideri, A. *J. Chem. Inf. Model.* **2016**, *56*, 941.

(30) Iacovelli, F.; Falconi, M.; Knudsen, B. R.; Desideri, A. *RSC Adv.* **2016**, *6*, 35160.

(31) Idili, A.; Plaxco, K. W.; Vallée-Bélisle, A.; Ricci, F. *ACS Nano* **2013**, *7*, 10863.

(32) Kandimalla, E. R.; Agrawal, S. *Gene* **1994**, *149*, 115.

(33) Kandimalla, E. R.; Manning, A.; Agrawal, S. *J. Biomol. Struct. Dyn.* **1996**, *14*, 79.

(34) Xodo, L. E.; Manzini, G.; Quadrifoglio, F. *Nucleic Acids Res.* **1990**, *18*, 3557.

(35) Frank-Kamenetskii, M. D.; Mirkin, S. M. *Annu. Rev. Biochem.* **1995**, *64*, 65.

(36) Lv, Y.; Hao, L.; Hu, W.; Ran, Y.; Bai, Y.; Zhang, L. *Sci. Rep.* **2016**, *6*, 29321.

(37) Hamelberg, D.; Mongan, J.; McCammon, J. A. *J. Chem. Phys.* **2004**, *120*, 11919.

(38) Santoro, M. M.; Bolen, D. W. *Biochemistry* **1988**, *27*, 8063.

(39) Myers, J. K. K.; Pace, C. N. N.; Scholtz, J. M. M. *Protein Sci.* **1995**, *4*, 2138.

(40) Lu, X. J.; Olson, W. K. *Nucleic Acids Res.* **2003**, *31*, 5108.

(41) DeLano, W. L. *PyMOL*; Schrödinger LLC, 2002, http://www.pymol.org, accessed January 20, 2017.

(42) Pettersen, E. F.; Goddard, T. D.; Huang, C. C.; Couch, G. S.; Greenblatt, D. M.; Meng, E. C.; Ferrin, T. E. *J. Comput. Chem.* **2004**, *25*, 1605.

(43) Salomon-Ferrer, R.; Case, D. A.; Walker, R. C. *Wiley Interdiscip. Rev. Comput. Mol. Sci.* **2013**, *3*, 198.

(44) Maier, J. A.; Martinez, C.; Kasavajhala, K.; Wickstrom, L.; Hauser, K. E.; Simmerling, C. *J. Chem. Theory Comput.* **2015**, *11*, 3696.

(45) Ivani, I.; Dans, P. D.; Noy, A.; Pérez, A.; Faustino, I.; Hospital, A.; Walther, J.; Andrio, P.; Goñi, R.; Balaceanu, A.; Portella, G.; Battistini, F.; Gelpí, J. L.; González, C.; Vendruscolo, M.; Laughton, C. A.; Harris, S. A.; Case, D. A.; Orozco, M. *Nat. Methods* **2015**, *13*, 55.

(46) Jorgensen, W. L.; Chandrasekhar, J.; Madura, J. D.; Impey, R. W.; Klein, M. L. *J. Chem. Phys.* **1983**, *79*, 926.

(47) Loncharich, R. J.; Brooks, B. R.; Pastor, R. W. *Biopolymers* **1992**, *32*, 523.

(48) Hardy, D. J.; Wu, Z.; Phillips, J. C.; Stone, J. E.; Skeel, R. D.; Schulten, K. *J. Chem. Theory Comput.* **2015**, *11*, 766.

DOI: 10.1021/jacs.6b11470
J. Am. Chem. Soc. 2017, 139, 5321−5329

(49) Ryckaert, J. P.; Ciccotti, G.; Berendsen, H. J. C. *J. Comput. Phys.* **1977**, *23*, 327.
(50) Feller, S. E.; Zhang, Y.; Pastor, R. W.; Brooks, B. R. *J. Chem. Phys.* **1995**, *103*, 4613.
(51) Pronk, S.; Páll, S.; Schulz, R.; Larsson, P.; Bjelkmar, P.; Apostolov, R.; Shirts, M. R.; Smith, J. C.; Kasson, P. M.; Van Der Spoel, D.; Hess, B.; Lindahl, E. *Bioinformatics* **2013**, *29*, 845.
(52) Abraham, M. J.; Murtola, T.; Schulz, R.; Páll, S.; Smith, J. C.; Hess, B.; Lindahl, E. *SoftwareX* **2015**, *1−2*, 19.
(53) Genheden, S.; Ryde, U. *Expert Opin. Drug Discovery* **2015**, *10*, 449.
(54) Roe, D. R.; Cheatham, T. E., III *J. Chem. Theory Comput.* **2013**, *9*, 3084.
(55) Miao, Y.; Sinko, W.; Pierce, L.; Bucher, D.; Walker, R. C.; Mccammon, J. A. *J. Chem. Theory Comput.* **2014**, *10*, 2677.
(56) Stadlbauer, P.; Trantírek, L.; Cheatham, T. E.; Koča, J.; Šponer, J. *Biochimie* **2014**, *105*, 22.
(57) Špačkova, N.; Cubero, E.; Šponer, J.; Orozco, M. *J. Am. Chem. Soc.* **2004**, *126*, 14642.
(58) Zuker, M. *Nucleic Acids Res.* **2003**, *31*, 3406.
(59) Zadeh, J. N.; Steenberg, C. D.; Bois, J. S.; Wolfe, B. R.; Pierce, M. B.; Khan, A. R.; Dirks, R. M.; Pierce, N. A. *J. Comput. Chem.* **2011**, *32*, 170.

DOI: 10.1021/jacs.6b11470
J. Am. Chem. Soc. 2017, 139, 5321−5329